The 9th European Congress on Computational Methods in Applied Sciences and Engineering
ECCOMAS Congress 2024
3 – 7 June 2024, Lisboa, Portugal

FINITE ELEMENT SIMULATION OF A RAINFALL INDUCED SHALLOW LANDSLIDE IN AN EXPERIMENTAL HILLSLOPE WITH A MULTIPHASE POROUS MEDIA MODEL

MARIA LAZARI[*], MATTEO CAMPORESE[*] AND LORENZO SANAVIA[*]

[*] University of Padua (UNIPD)
Department of Civil Environmental and Architectural Engineering
via F. Marzolo 9, 35131 Padova, Italy
e-mail: maria.lazari@unipd.it, matteo.camporese@unipd.it, lorenzo.sanavia@unipd.it,
www.dicea.unipd.it

Key words: Rainfall-triggered slope instability, Generalized Plasticity, Variably saturated porous media, Large scale physical model, FEM.

Summary. This study presents the results of a FEM numerical simulation of a large scale physical model of a slope subjected to rainfall infiltration. The slope failure is modelled as a coupled variably saturated thermo-hydro-mechanical problem, using the Pastor-Zienkiewicz generalised plasticity model to obtain the soil's mechanical response. Small strain and quasi-static loading conditions are assumed, and plane strain conditions are adopted in the slope stability analysis. The hydraulic and mechanical parameters are calibrated based on the available experimental data. The numerical results are compared with the experimental data of the mechanical and the hydraulic responses up to failure.

1 INTRODUCTION

Heavy rainfall can trigger a slope failure in the case, for example, of a shallow soil deposit of different grading and origin, which is in a state of partial saturation. In this type of slope instability, the slope failure is associated with changes in the pore-water pressure, the retention properties and the stress state during rainfall infiltration, as well as with changes in the soil properties caused by the progressive water infiltration [1], which involves both mechanical and hydrological processes.

In order to understand these key physical processes, a large-scale physical model of a slope is tested. The slope comprised a shallow upper layer of fine loose sand overlying a well-compacted sandy clay bed. Sensors and optical fibres were introduced within the upper layer to monitor the pore water pressure, the moisture content and the strain [2, 3]. Rainfall was artificially applied by a system of nozzles with drops of a small diameter to avoid surface erosion [2]. During rainfall, a wetting front moved downward reaching the interface with the sandy clay bed. This led to saturation of the upper soil layer, resulting in an increase of pore water pressure. The increase in pore pressure resulted in a reduction in effective stress, which in turn diminished the shear strength of the soil. This ultimately resulted in slope failure at the interface between the two soils [3].

Herein, the rainfall induced slope failure is modelled as a coupled variably saturated thermo-hydro-mechanical problem using the geometrically linear finite element code Comes-Geo [4]. The problem is solved in the quasi-static [5] regime using Taylor-Hood finite elements [6-7]. For the loose sand layer, the Pastor-Zienkiewicz generalised plasticity model [8] is used, in which yield and plastic potential surfaces are not explicitly required. The comparison between the experimental and the numerical results is presented, showing the capability of the numerical model to describe the experimental results and provide us with an insight of the triggering mechanisms during the progressive failure of the experimental slope.

This work aims to emphasize the importance of the multiphase modelling for the simulation of the hydro-mechanical behaviour of variably saturated slopes, as a useful numerical tool for the development of landslide early warning systems.

In the following, we first summarize the mathematical and finite element model for multiphase geomaterials. Then a short description of the experiment along with the numerical modelling follows. Finally, the results of the thermo-hydro-mechanical analysis are presented and discussed.

The interested reader will found in [26] the results of the full numerical simulation of the experimental slope of this work extending the model adopted here to dynamics, using for the loose sand layer the Bolzon-Schrefler constitutive model for non-isothermal variably saturated sands, studying the instability of the slope using the local and global Hill sufficient stability criterion and comparing the numerical results with the following measured data: water content in six WCR, water pressure in six TDR, water outflow at the toe of the slope and axial strain and temperature at the interface between the sand layer and the sandy clay bed.

2 MATHEMATICAL MODEL

The mathematical model necessary to simulate the thermo-hydro-mechanical behaviour of fully and partially saturated porous media is developed within the Hybrid Mixture Theory [4], [9] using the averaging theories by [10-12]. For sake of brevity only a general description of the mathematical framework of the model with its basic assumptions will be presented hereafter.

The variably saturated porous medium, such as a slope, is treated as a multiphase system consisting of a solid skeleton with open pores filled with liquid water and gas. The gas phase is modelled as an ideal gas composed of dry air (non-condensable gas) and water vapour (condensable gas), which are considered as two miscible species. Phase changes of water (evaporation and condensation) as well as heat transfer through conduction and convection are considered. All fluid phases are in contact with the solid phase and the solid is deformable resulting in coupling of the fluid, the solid and the thermal fields. In the partially saturated zones the liquid water is separated from its vapour by a concave meniscus (capillary water). Due to the curvature of this meniscus, the sorption equilibrium equation [13] gives the relationship, $p^c = p^g - p^w$ between the capillary pressure p^c (also known as matric suction), gas pressure p^g and liquid water pressure p^w.

The final model consists of four balance equations: mass balance of the dry air, mass balance of water species, enthalpy of the whole medium and the equilibrium equation of the multiphase medium. They are completed with appropriate constitutive equations for fluids

and solid phases. The balance equations were developed in geometrically linear framework and are written in this paper at the macroscopic level considering quasi-static loading conditions [5]. The chosen state variables are: gas pressure p^g, capillary pressure p^c, temperature T and the displacement vector of solid matrix **u**.

In the following, direct notation will be adopted. Boldface letters will denote vector or tensors and lightface italic letters will be used for scalar quantities.

2.1 Governing equations

The equilibrium equation of the mixture in terms of generalized effective Cauchy's stress tensor $\boldsymbol{\sigma}'(\boldsymbol{x}, t)$ [4] assumes the form:

$$\operatorname{div}\left(\boldsymbol{\sigma}' - \left[p^g - S_w p^c \right]\mathbf{1}\right) + \rho\mathbf{g} = 0 \tag{1}$$

where $\rho = [1-n]\rho^s + nS_w\rho^w + nS_g\rho^g$ is the mass density of the overall medium, $n(\boldsymbol{x}, t)$ is the porosity, $S_w(\boldsymbol{x}, t)$ and $S_g(\boldsymbol{x}, t)$ are respectively the water and gas degree of saturation, **g** is the gravity acceleration vector and **1** is the second order identity tensor.

The mass conservation equation for the mixture of solid skeleton, liquid water and its vapour is:

$$\begin{aligned} & n\left[\rho^w - \rho^{gw}\right]\left[\frac{\partial S_w}{\partial t}\right] + \left[\rho^w S_w + \rho^{gw}\left[1 - S_w\right]\right]\operatorname{div}\left(\frac{\partial \mathbf{u}}{\partial t}\right) \\ & + \left[1 - S_w\right] n \frac{\partial \rho^{gw}}{\partial t} - \operatorname{div}\left(\rho^g \frac{M_\alpha M_w}{M_g^2} \boldsymbol{D}_{\mathrm{g}}^{\mathrm{gw}} \operatorname{grad}\left(\frac{p^{gw}}{p^g}\right)\right) \\ & + \operatorname{div}\left(\rho^w \frac{\mathbf{k}^{\mathrm{w}} k^{rw}}{\mu^w}\left[-\operatorname{grad}(p^g) + \operatorname{grad}(p^c) + \rho^w \mathbf{g}\right]\right) \\ & + \operatorname{div}\left(\rho^{gw} \frac{\mathbf{k}^{\mathrm{g}} k^{rg}}{\mu^g}\left[-\operatorname{grad}(p^g) + \rho^g \mathbf{g}\right]\right) - \beta_{swg}\frac{\partial T}{\partial t} = 0 \end{aligned} \tag{2}$$

where $\mathbf{k}^\pi(\boldsymbol{x}, t) = k^\pi(\boldsymbol{x}, t)\mathbf{1}$ is the intrinsic permeability tensor of the porous matrix in π-fluid saturated condition [m^2], which is assumed to be isotropic, $k^{r\pi}(\boldsymbol{x},t)$ is the fluid relative permeability parameter and $\mu^\pi(\boldsymbol{x}, t)$ is the dynamic viscosity of the fluid, with $\pi = w, g$. $\boldsymbol{D}_{\mathrm{g}}^{\mathrm{gw}}$ is the effective diffusivity tensor of water vapour in the gas phase contained within the pore space, $\beta_{swg} = \beta_s(1-n)\cdot(S_g\,\rho^{gw} + \rho^w S_w)$ and M_a, M_w and $M_g(\boldsymbol{x},t)$ are the molar mass of dry air, liquid water and gas mixture, respectively.

Similarly, the mass balance equation for the dry air is:

$$\begin{aligned} & -n\rho^{g\alpha}\left[\frac{\partial S_w}{\partial t}\right] + \rho^{g\alpha}\left[1 - S_w\right]\operatorname{div}\left(\frac{\partial \mathbf{u}}{\partial t}\right) + n\left[1 - S_w\right]\frac{\partial \rho^{g\alpha}}{\partial t} - \operatorname{div}\left(\rho^g \frac{M_\alpha M_w}{M_g^2} \mathbf{D}_{\mathrm{g}}^{\mathrm{g}\alpha} \operatorname{grad}\left(\frac{p^{g\alpha}}{p^g}\right)\right) \\ & + \operatorname{div}\left(\rho^{g\alpha} \frac{\mathbf{k}^{\mathrm{g}} k^{rg}}{\mu^g}\left[-\operatorname{grad}(p^g) + \rho^g \mathbf{g}\right]\right) - \left[1 - n\right]\beta_s \rho^{g\alpha}\left[1 - S_w\right]\frac{\partial T}{\partial t} = 0 \end{aligned} \tag{3}$$

The enthalpy balance equation of the mixture has the following form:

$$\left(\rho C_p\right)_{eff}\frac{\partial T}{\partial \mathrm{t}}+\rho^w C_p^w\left[\frac{\mathbf{k}^{\mathrm{w}}k^{rw}}{\mu^w}\left[-\mathrm{grad}(p^g)+\mathrm{grad}(p^c)+\rho^w\mathbf{g}\right]\right]\cdot\mathrm{grad}T$$
$$+\rho^g C_p^g\left[\frac{\mathbf{k}^g k^{rg}}{\mu^g}\left[-\mathrm{grad}(p^g)+\rho^g\mathbf{g}\right]\right]\cdot\mathrm{grad}T-\mathrm{div}\left(\chi_{eff}\,\mathrm{grad}T\right)=-\dot{\mathrm{m}}_{\mathrm{vap}}\Delta\mathrm{H}_{\mathrm{vap}} \tag{4}$$

where, $\rho(C_p)_{eff}$ is the effective thermal capacity of the porous medium, $C_p^w(\boldsymbol{x},t)$ and $C_p^g(\boldsymbol{x},t)$ are the specific heat of the water and gas mixture respectively, and $\chi_{eff}(\boldsymbol{x}, t)$ is the effective thermal conductivity of the porous medium. The right hand side term of Eq. (4) considers the contribution of the evaporation and condensation.

2.2 Constitutive equations

To complete the description of the mechanical behaviour, constitutive equations have to be specified. For the gas phase which is assumed to be a perfect mixture of two ideal gases, the state equation of a perfect gas (Clapeyron's equation) and Dalton's law are applied to dry air ($g\alpha$), water vapour (gw) and moist air (g). In the partially saturated zones, the water vapour pressure $p^{gw}(\boldsymbol{x}, t)$ is obtained from the Kelvin-Laplace equation. The saturation $S_\pi(\boldsymbol{x}, t)$ and the relative permeability $k^{r\pi}(\boldsymbol{x},t)$ are experimentally determined functions of the capillary pressure p^c and the temperature T.

The behaviour of the solid skeleton is described within the framework of Generalized Plasticity [14] and in particular with the Pastor-Zienkiewicz constitutive model [15]. In order to introduce the dependency on the increment of stress tensor, a direction n discriminating between states of loading (L) and unloading (U) is introduced as:

$$\mathrm{d}\boldsymbol{\varepsilon}=\mathbf{C}^L:\mathrm{d}\boldsymbol{\sigma},\quad \mathbf{n}:\mathrm{d}\boldsymbol{\sigma}^e>0\rightarrow\text{loading}$$
$$\mathrm{d}\boldsymbol{\varepsilon}=\mathbf{C}^U:\mathrm{d}\boldsymbol{\sigma},\quad \mathbf{n}:\mathrm{d}\boldsymbol{\sigma}^e<0\rightarrow\text{unloading} \tag{5}$$

where $\mathrm{d}\boldsymbol{\sigma}^e$ is the elastic stress increment obtained if the material behaved elastically. The neutral loading corresponds to the limit case for which $\mathbf{n}$:$\mathrm{d}\boldsymbol{\sigma}^e$=0. Continuity between loading and unloading processes requires the constitutive tensors for loading and unloading should be of the form:

$$\mathbf{C}^L=\mathbf{C}^e+\frac{1}{H_L}\mathbf{n}_{gL}\otimes\mathbf{n}$$
$$\mathbf{C}^U=\mathbf{C}^e+\frac{1}{H_U}\mathbf{n}_{gU}\otimes\mathbf{n} \tag{6}$$

where $\mathbf{C}^e$ is a fourth-order tensor characterizing the elastic behaviour of the material, $\mathbf{n}_{gL/U}$ are two unit tensors defining the plastic flow direction in loading (L) and unloading (U) and $H_{L/U}$ are two scalar functions defined as loading (L) and unloading (U) plastic modulus. From Eq. (6) it follows that the total strain increments can be divided into elastic and plastic components, as:

$$\mathrm{d}\boldsymbol{\varepsilon} = \mathrm{d}\boldsymbol{\varepsilon}^e + \mathrm{d}\boldsymbol{\varepsilon}^p$$
$$\mathrm{d}\boldsymbol{\varepsilon}^e = \mathbf{C}^e : \mathrm{d}\boldsymbol{\sigma}, \quad \mathrm{d}\boldsymbol{\varepsilon}^p = \frac{1}{H_{L/U}} (\mathbf{n}_{gL/U} \otimes \mathbf{n}) : \mathrm{d}\boldsymbol{\sigma} \tag{7}$$

Therefore, to fully characterize the material behaviour within a generalized plasticity approach, the following items need to be provided [16]: the elastic constitutive tensor $\mathbf{C}^e$, the unit tensor $\mathbf{n}$ discriminating loading and unloading conditions, the unit tensor describing the direction of plastic flow $\mathbf{n}_{gL/U}$ in loading and unloading and finally the loading and unloading plastic moduli $H_{L/U}$.

Elasticity

The model assumes a non-linear elastic response of soils, in which the bulk modulus K and the shear modulus G consider pressure-dependence, according to the following relationships:

$$K = K_{ref} \frac{p'}{p'_{ref}} \qquad G = G_{ref} \frac{p'}{p'_{ref}} \tag{8}$$

where K_{ref} and G_{ref} are material parameters at the reference mean effective stress, p'_{ref}

Loading and unloading directions

The plastic strain direction unit tensor in loading is defined in the triaxial space as [15]:

$$\mathbf{n}_{gL}^{\mathrm{T}} = \left\{\mathbf{n}_{gv}, \mathbf{n}_{gs}\right\} = \frac{1}{\sqrt{1 + d_g^2}} \left\{d_g, 1\right\} \tag{9}$$

where the dilatancy term d_g, defined as the ratio between the increments of plastic volumetric and shear strain, is given by:

$$d_g = (1 + a)\left(M_g - \eta\right) \tag{10}$$

and M_g and α are material parameters. In this expression, the term M_g corresponds to the slope of the critical state line in the $\{p',q\}$ plane under triaxial compression. Dilatancy is zero at the line $\eta = M_g$ where η is the stress ratio q/p'. During unloading, plastic strain direction unit tensor $\mathbf{n}_{gU}$ is provided by [15]:

$$\begin{aligned} \mathbf{n}_{gU} &= \left\{\mathbf{n}_{gUv}, \mathbf{n}_{gUs}\right\}^{\mathrm{T}} \\ \mathbf{n}_{gUv} &= -abs(\mathbf{n}_{gv}) \\ \mathbf{n}_{gUs} &= +\mathbf{n}_{gs} \end{aligned} \tag{11}$$

For non-associative flow rule, direction $\mathbf{n}$ should be specified as different from $\mathbf{n}_{gL}$:

$$\mathbf{n}^{\mathrm{T}} = \left\{\mathbf{n}_v, \mathbf{n}_s\right\} = \frac{1}{\sqrt{1 + d_f^2}} \left\{d_f, 1\right\} \tag{12}$$

where d_f is given by:

$$d_f = (1+a)\left(M_f - \eta\right) \tag{13}$$

The associative behaviour is recovered by setting $M_g = M_f$.

Plastic modulus

The plastic modulus, which is postulated directly without introducing any hardening law and consistency condition [15], is:

$$H_L = H_0 p' \tilde{H}_f \left(\tilde{H}_v + \tilde{H}_s\right) \tilde{H}_{Dm} \tag{14}$$

In the above equation H_0 is a multiplying factor related to plastic strains at the beginning of the loading process, H_s is a function of the accumulated plastic deviatoric strain and H_v refers to the volumetric strain hardening:

$$\tilde{H}_s = \beta_0 \beta_1 \exp\left(-\beta_0 \xi\right) \qquad \tilde{H}_v = \left(1 - \frac{\eta}{M_g}\right) \tag{15}$$

The equation for H_f is:

$$\tilde{H}_f = \left(1 - \frac{\eta}{\eta_f}\right)^4, \qquad \eta_f = \left(1 + \frac{1}{a}\right) M_f \tag{16}$$

H_{Dm} is a function that incorporates material memory:

$$\tilde{H}_{Dm} = \left(\frac{\zeta_{max}}{\zeta}\right)^{\gamma} \tag{17}$$

in which ζ is the mobilized stress function defined as:

$$\zeta = p' \left[1 - \left(\frac{\alpha}{1+\alpha}\right) \frac{\eta}{M_f}\right]^{-1/\alpha} \tag{18}$$

The definition of the coefficients of the Pastor-Zienkiewicz model can be found in [17].

2.3 Finite element formulation

The model described above has been implemented in the finite element code for multiphase porous media Comes-Geo, developed at the University of Padova (i.e. [4, 5], [18-22]). The finite element model is derived by applying the Galerkin procedure for the spatial integration with different order of interpolation functions for solid displacements (biquadratic) and fluid pressures/temperature (bilinear), and the Generalized Trapezoidal Method for the time integration of the weak form of the balance equations summarized in the previous section. Details concerning the matrices and the residual vector of the linearized equations system of the finite element model can be found in [5].

3 NUMERICAL SIMULATION OF AN EXPERIMENTAL HILLSLOPE SUBJECTED TO RAINFALL

3.1 The experimental hillslope and model setup

The experiment which was carried out in the University of Padova [3], considers a slope failure triggered by rainfall infiltration. It was carried out on a large-scale physical model of a slope built inside a 6 x 2 m reinforced concrete container structure (Figure 1a). The slope toe consists of a porous wall made of hollow bricks, allowing water to discharge. The slope consists of two soil layers: a constant thickness layer of permeable soil made of fine loose sand, overlaying a less permeable, well-compacted sandy clay. The artificial rainfall with a steady intensity of 160 mm/h is applied on the slope surface until the slope collapse.

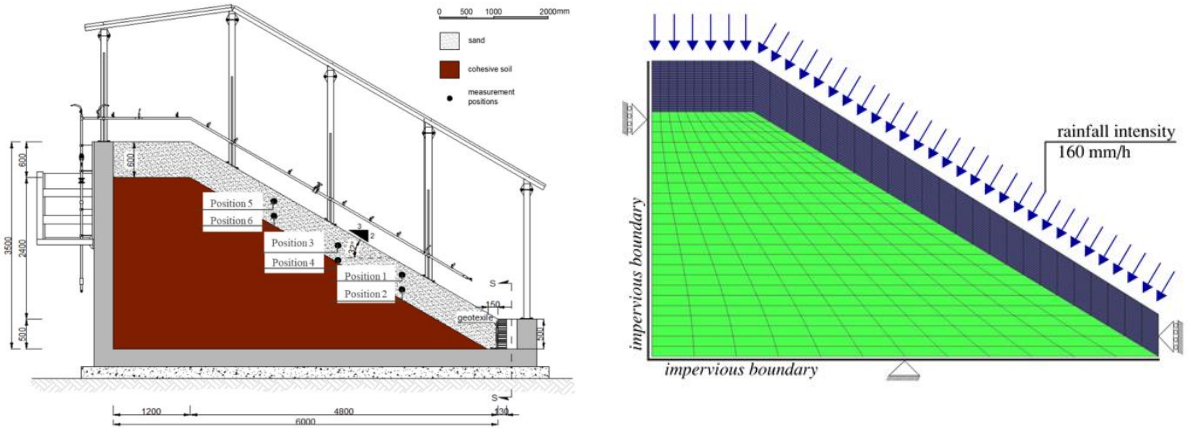

(a) (b)

Figure 1: (a) Geometry, soil layers and monitoring points of the experimental model [2] and (b) finite element mesh of the numerical model and boundary conditions.

In Figure 1b the finite element model of the slope is presented along with the applied boundary conditions. The mesh is composed of 1008 eight-node quadrilateral Taylor-Hood elements and plane strain conditions are assumed. The vertical and horizontal displacements are constrained at the bottom surface while only the horizontal displacements are constrained at the lateral surfaces. Initially, the stress state is computed in equilibrium with the gravity load and the initial conditions. Then, rainfall infiltration is simulated by means of an imposed boundary flux of 160 mm/h along the upper surface. The left and bottom boundaries are considered impermeable, the upper and sloped boundary are at atmospheric pressure, while the toe is a seepage face boundary [23].

The mechanical material properties for the loose sand layer are mainly derived from the experimental results taken from [24], and are summarized in Table 1. For the water degree of saturation and the water relative permeability, van Genuchten relations [25] are used and the parameters for the curves can be found in [24].

Table 1: Model parameters for the loose sand layer.

Parameter	Value
E [MPa]	4.0
v [-]	0.3
n [-]	0.5
ρ^s [kg/m^3]	2718
M_g [-]	1.35
M_f [-]	0.5
$a_g = a_f$ [-]	0.45
β_0 [-]	2.25
β_1 [-]	0.2
H_0 [-]	4000

3.2 Results

Figure 2 and Figure 3 show the comparison of the experimental data with the numerical results as a function of time from the beginning of rainfall. Results are presented at two different positions along the slope for the pore water pressure and the volumetric water content. As shown from the volumetric water content the slope is gradually driven to saturation through vertical water flow. A first sharp increase in pore water pressure and volumetric water content is observed in the uppermost positions (i.e. position 1) followed by the deeper ones (i.e. position 2). The infiltration front propagates from the top surface of the slope to the interface of the two soil layers. Only a small fraction of the infiltrating water is absorbed by the less permeable clay layer. The positive values of pore water pressure for the deeper sensor indicates the development of saturated front moving upwards until the formation of a perched water table that gradually rises to the top of the slope as shown in Figure 4a. With increasing water content the capillary force acting between the soil particles decreases, leading to loss of strength for the soil and finally to the slope collapse at 135 min, that is approximately the actual time of the failure of the experiment.

It is observed that the model is able to capture this behaviour and the numerical results are in excellent agreement with the experimental data both in terms of pore water pressure and volumetric water content.

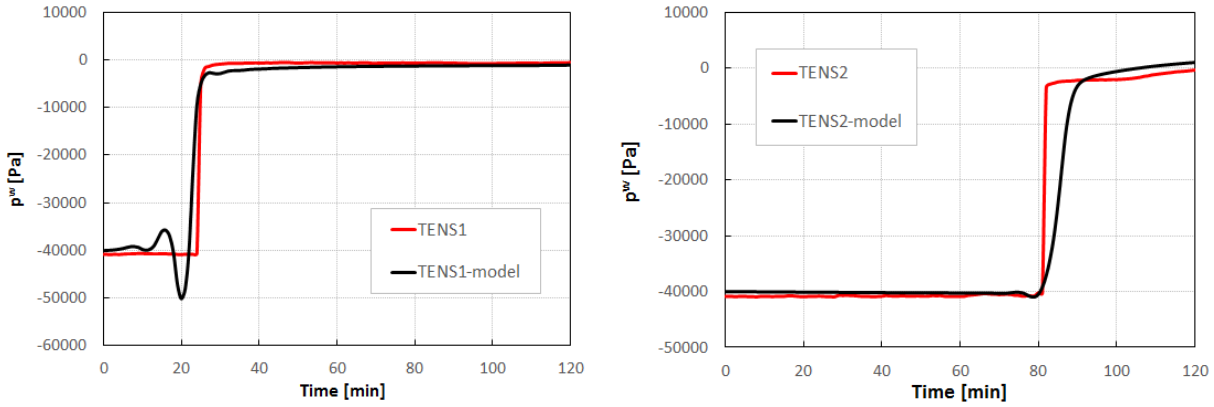

Figure 2: Comparison between the numerical and experimental pore water pressure, p^w, at positions 1 and 2.

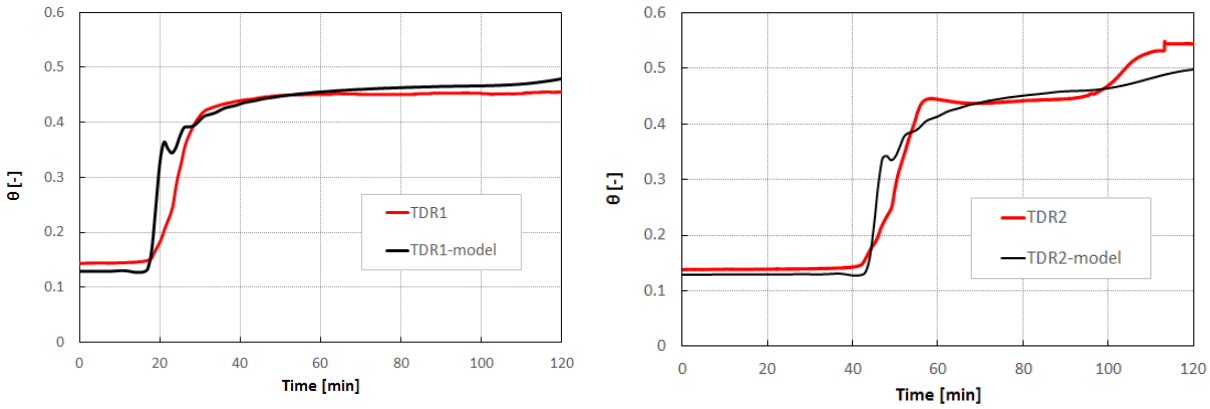

Figure 3: Comparison between the numerical and experimental volumetric water content, θ, at positions 1 and 2.

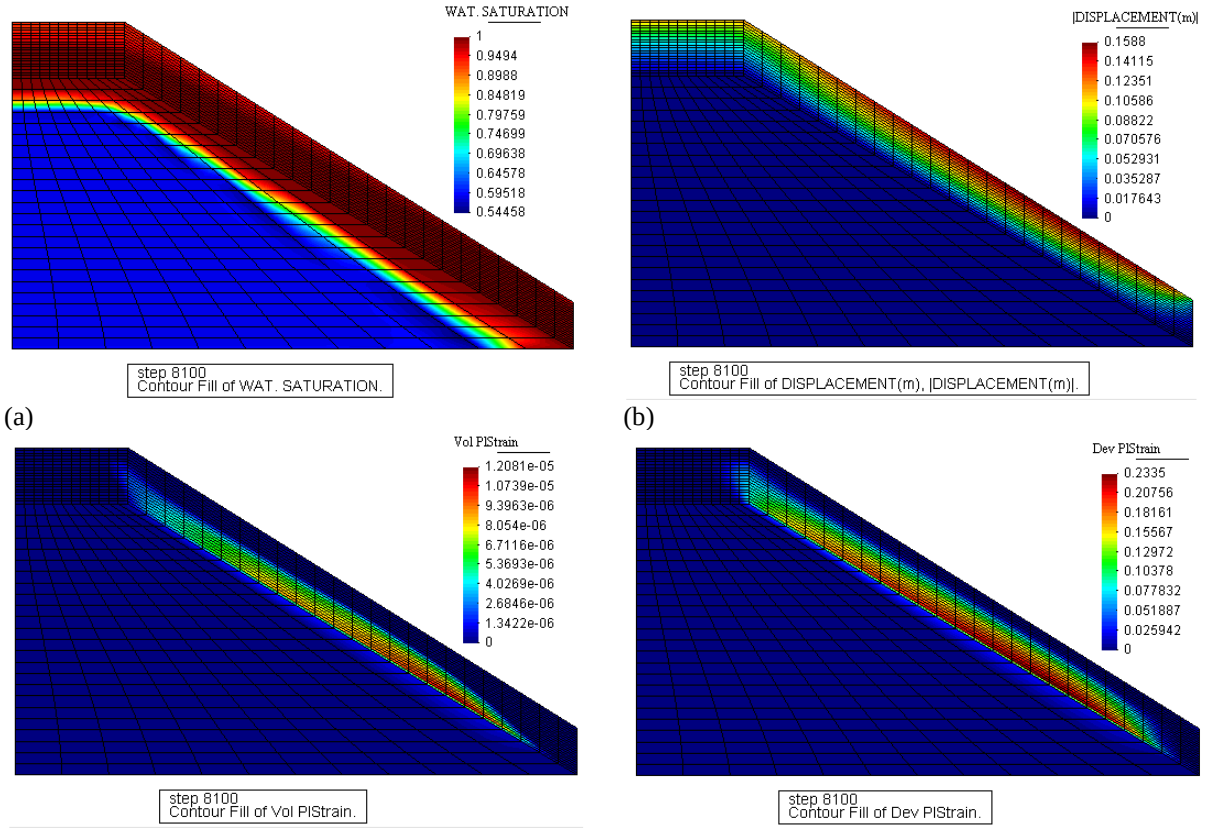

Figure 4: Contours of a) water degree of saturation, (b) displacements, (c) volumetric plastic strain and (d) deviatoric plastic strain at failure (135min).

The distribution of displacements along the slope at failure is depicted in Figure 4b. The soil top surface develops higher displacement as the material fails and slides towards the toe of the slope, in consistency with the failure profile of the experiment.

The distribution and the development of the deviator plastic strain as well as volumetric

plastic strain are presented in Figure 4c, d respectively. The plastic strains at failure are bounded to the upper and mid-lower part of the slope, where mobilization, dilatancy and sliding of the material occurred without reaching the toe, and the maximum values mainly concentrate close to the interface between the two layers. This behaviour was also observed in the experiment [3].

4 CONCLUSIONS

In this paper, the finite element analysis of a large-scale experimental slope subjected to rainfall is considered as a coupled variably saturated thermo-hydro-mechanical problem. A multiphase model is used in conjunction with the Pastor-Zienkiewicz model for the soil. Thermal effects are negligible and the problem is solved assuming quasi-static loading conditions. The examination of both pore water pressure and volumetric water content revealed that the increase in pore pressures triggered the slope collapse at the interface between the two soil layers, with slope failure occurring approximately at the actual time of failure in the experiment. It is shown that the numerical model can predict the experimental observations very well, both in terms of the hydraulic and mechanical behaviour, highlighting the importance of multiphase modelling in the analysis and prediction of landslide phenomena.

5 ACKNOWLEDGMENTS

The authors wish to thank the 7th Framework Programme of the European Union (ITN MuMoLaDe project 289911) and the University of Padova (BIRD208040) for financially supporting this work.

REFERENCES

[1] Zhang, Z., Zeng, R., Meng, X., Zhao, S., Wang, S., Ma, J. and Wang, H. 2023. “Effects of changes in soil properties caused by progressive infiltration of rainwater on rainfall-induced landslides.” Catena, 233, 107475. https://doi.org/10.1016/j.catena.2023.107475

[2] Lora, M., Camporese, M., Troch, P.A. and Salandin, P. 2016. “Rainfall-triggered shallow landslides: infiltration dynamics in a physical hillslope model.” Hydrological Processes 30, 3239–3251. https://doi.org/10.1038/s41598-017-12610-1

[3] Schenato, L., Palmieri, L., Camporese, M., Bersan, S., Cola, S., Pasuto, A., Galtarossa, A., Salandin, P. and Simonini, P. 2017. “Distributed optical fibre sensing for early detection of shallow landslides triggering.” Scientific Reports, 7, 14686. https://doi.org/10.1038/s41598-017-12610-1

[4] Lewis, R.W. and Schrefler, B.A. 1998. *The Finite Element Method in the Static and Dynamic Deformation and Consolidation of Porous Media*. John Wiley, New York.

[5] Sanavia, L., Pesavento, F. and Schrefler, B.A. 2006. “Finite element analysis of non-isothermal multiphase geomaterials with application to strain localisation simulation.” Computational Mechanics, 37 (4), 331-348. https://doi.org/10.1007/s00466-005-0673-6

[6] Cao, T. D., Sanavia, L., and Schrefler, B.A. 2016. "A thermo-hydro-mechanical model for multiphase geomaterials in dynamics with application to strain localization simulation." International Journal for Numerical Methods in Engineering, 107, 312–337. https://doi.org/10.1002/nme.5175

[7] Sanavia, L. and Cao, D.T. 2017. Modelling multiphase geomaterials at high temperatures in dynamics with application to strain localization and rapid catastrophic landslides. *Poromechanics VI: Proceedings of the Sixth Biot Conference on Poromechanics*. July 9-13, 2017, Paris, (F). Edited by Matthieu Vandamme; Patrick Dangla; Jean-Michel Pereira and Siavash Ghabezloo. 1866-1875. https://doi.org/10.1061/9780784480779.231

[8] Pastor, M., Zienkiewicz, O.C., and Chan, A.H.C. 1990. "Generalized plasticity and the modelling of soil behaviour." International Journal for Numerical and Analytical Methods in Geomechanics, 14, 151–190. https://doi.org/10.1002/nag.1610140302

[9] Schrefler, B.A. 2002. "Mechanics and thermodynamics of saturated/unsaturated porous materials and quantitative solutions." Applied Mechanics Reviews, 55(4), 351-388. https://doi.org/10.1115/1.1484107

[10] Hassanizadeh, M. and Gray, W.G. 1979a. "General conservation equations for multi-phase system: 1. Averaging technique." Advances in Water Resources, 2, 131-144.

[11] Hassanizadeh, M. and Gray, W.G. 1979b. "General conservation Equations for multi-phase system: 2. Mass, momenta, energy and entropy equations." Advances in Water Resources, 2, 191-201.

[12] Hassanizadeh, M. and Gray, W.G. 1980. "General conservation equations for multi-phase systems: 3. Constitutive theory for porous media flow." Advances in Water Resources, 3(1), 25-40.

[13] Gray, W.G. and Hassanizadeh, M. 1991. "Unsaturated flow theory including interfacial phenomena." Water Resources Research, 27, 1855-1863. https://doi.org/10.1029/91WR01260

[14] Zienkiewicz, O.C. and Mroz, Z. 1984. *Generalized plasticity formulation and applications to Geomechanics.* Mechanics of Engineering Materials, Desai C.S. and Gallagher R.H. (eds), 33, 655-679, Wiley, New York.

[15] Pastor, M., Zienkiewicz, O.C. and Chan, A.H.C. 1990. "Generalized plasticity and the modelling of soil behaviour." International Journal for Numerical and Analytical Methods in Geomechanics, 14, 151-190. https://doi.org/10.1002/nag.1610140302

[16] Manzanal, D., Merodo, J.A.F. and Pastor, M. 2011. "*Generalized plasticity state parameter-based model for saturated and unsaturated soils. Part 1: Saturated state.*"

International Journal for Numerical and Analytical Methods in Geomechanics, 35, 1347-1362. https://doi.org/10.1002/nag.961

[17] Chan, A.H.C., Pastor, M., Schrefler, B.A., Shiomi, T. and Zienkiewicz, O.C. 2022. *Computational Geomechanics: Theory and Applications*, Second Edition, John Wiley & Sons, New York.

[18] Sanavia, L. 2009. "Numerical modelling of a slope stability test by means of porous media mechanics." Engineering Computations, 26(3), 245-266. https://doi.org/10.1108/02644400910943608

[19] Gawin, D. and Sanavia, L. 2010. "Simulation of cavitation in water saturated porous media considering effects of dissolved air." Transport Porous Media, 81:141-160. https://doi.org/10.1007/s11242-009-9391-4

[20] Sanavia, L., François, B., Bortolotto, B., Luison, L. and Laloui, L. 2008. "Finite element modelling of thermo-elasto-plastic water saturated porous materials." Journal of Theoretical and Applied Mechanics, 38, 7-24.

[21] Lazari, M., Sanavia, L. and Schrefler, B.A. 2015. "Local and non-local elasto-viscoplasticity in strain localization analysis of multiphase geomaterials." International Journal for Numerical and Analytical Methods in Geomechanics, 39(14), 1570-1592. https://doi.org/10.1002/nag.2408

[22] Lazari, M., Sanavia, L., di Prisco, C. and Pisanó, F. 2018. "Predictive potential of Perzyna viscoplastic modelling for granular geomaterials." International Journal for Numerical and Analytical Methods in Geomechanics, 43(2), 544-1567. https://doi.org/10.1002/nag.2876

[23] Scudeler, C., Paniconi, C., Pasetto, D. and Putti M. 2017. "Examination of the seepage face boundary condition in subsurface and coupled surface/subsurface hydrological models." Water Resources Research, 53, 1799–1819. https://doi.org/10.1002/2016WR019277

[24] Cavallaro, M. 2016. *Modellazione fisica e numerica dei processi idrologici di innesco delle frane superficiali*, PhD. Thesis, University of Padova, Italy.

[25] van Genuchten, M.Th. 1980. "A Closed-form Equation for Predicting the Hydraulic Conductivity of Unsaturated Soils." Soil Science Society of America Journal, 44(5), 892-898.

[26] Lazari, M., Camporese, M. and Sanavia, L. (under revision). "Multphase and multiphysics modelling of a rainfall induced failure in an experimental hillslope."